frontiers in Immunology

ORIGINAL RESEARCH
published: 31 March 2022
doi: 10.3389/fimmu.2022.805076

Emergent Temporal Signaling in Human Trabecular Meshwork Cells: Role of TRPV4-TRPM4 Interactions

Oleg Yarishkin[1†], Tam T. T. Phuong[1†], Felix Vazquez-Chona[1], Jacques Bertrand[2], Joseph van Battenburg-Sherwood[2], Sarah N. Redmon[1], Christopher N. Rudzitis[1,3], Monika Lakk[1], Jackson M. Baumann[1,4], Marc Freichel[5], Eun-Mi Hwang[6], Darryl Overby[2] and David Križaj[1,3,4,7]*

[1] Department of Ophthalmology and Visual Sciences, University of Utah School of Medicine, Salt Lake City, United States, [2] Department of Bioengineering, Imperial College London, London, United Kingdom, [3] Interdepartmental Program in Neuroscience, University of Utah, Salt Lake City, United States, [4] Department of Bioengineering, University of Utah, Salt Lake City, United States, [5] Institute of Pharmacology, Heidelberg University, Heidelberg, Germany, [6] Center for Functional Connectomics, Korea Institute of Science and Technology (KIST), Seoul, South Korea, [7] Department of Neurobiology, University of Utah, Salt Lake City, United States

OPEN ACCESS

Edited by:
Ruchi Bansal,
University of Twente, Netherlands

Reviewed by:
Günther Schlunck,
University of Freiburg, Germany
Jonathan Soboloff,
Temple University, United States

***Correspondence:**
David Križaj
david.krizaj@hsc.utah.edu

†These authors have contributed equally to this work

Specialty section:
This article was submitted to Molecular Innate Immunity, a section of the journal Frontiers in Immunology

Received: *29 October 2021*
Accepted: *02 March 2022*
Published: *31 March 2022*

Citation:
Yarishkin O, Phuong TTT, Vazquez-Chona F, Bertrand J, van Battenburg-Sherwood J, Redmon SN, Rudzitis CN, Lakk M, Baumann JM, Freichel M, Hwang EM, Overby D and Križaj D (2022) Emergent Temporal Signaling in Human Trabecular Meshwork Cells: Role of TRPV4-TRPM4 Interactions. Front. Immunol. 13:805076. doi: 10.3389/fimmu.2022.805076

Trabecular meshwork (TM) cells are phagocytic cells that employ mechanotransduction to actively regulate intraocular pressure. Similar to macrophages, they express scavenger receptors and participate in antigen presentation within the immunosuppressive milieu of the anterior eye. Changes in pressure deform and compress the TM, altering their control of aqueous humor outflow but it is not known whether transducer activation shapes temporal signaling. The present study combines electrophysiology, histochemistry and functional imaging with gene silencing and heterologous expression to gain insight into Ca^{2+} signaling downstream from TRPV4 (Transient Receptor Potential Vanilloid 4), a stretch-activated polymodal cation channel. Human TM cells respond to the TRPV4 agonist GSK1016790A with fluctuations in intracellular Ca^{2+} concentration ($[Ca^{2+}]_i$) and an increase in $[Na^+]_i$. $[Ca^{2+}]_i$ oscillations coincided with monovalent cation current that was suppressed by BAPTA, Ruthenium Red and the TRPM4 (Transient Receptor Potential Melastatin 4) channel inhibitor 9-phenanthrol. TM cells expressed TRPM4 mRNA, protein at the expected 130-150 kDa and showed punctate TRPM4 immunoreactivity at the membrane surface. Genetic silencing of TRPM4 antagonized TRPV4-evoked oscillatory signaling whereas TRPV4 and TRPM4 co-expression in HEK-293 cells reconstituted the oscillations. Membrane potential recordings suggested that TRPM4-dependent oscillations require release of Ca^{2+} from internal stores. 9-phenanthrol did not affect the outflow facility in mouse eyes and eyes from animals lacking TRPM4 had normal intraocular pressure. Collectively, our results show that TRPV4 activity initiates dynamic calcium signaling in TM cells by stimulating TRPM4 channels and intracellular Ca^{2+} release. It is possible that TRPV4-TRPM4 interactions downstream from the tensile and compressive impact of intraocular pressure contribute to homeostatic regulation and pathological remodeling within the conventional outflow pathway.

Keywords: Trabecular meshwork, TRPV4, TRPM4, calcium oscillations, glaucoma, conventional outflow facility, GSK1016790, immune

INTRODUCTION

Biomechanical factors such as intraocular pressure (IOP) are an important determinant of the ocular environment, with roles in growth, cellular signaling that subserve ocular health and pathology (1). IOP is homeostatically regulated by the trabecular meshwork (TM), a mechanosensitive phagocytic tissue composed of smooth muscle-, macrophage- and fibroblast-like cells that function as an adaptive valve for outflow of aqueous humor from the anterior eye (1, 2). In healthy cells, acute IOP elevations engender an increase in outflow resistance that is followed by an adaptive response that guides gradual recovery of tissue permeability to fluid flow (3) whereas chronic mechanical stress triggers transdifferentiation of TM cells into stiff and contractile myofibroblasts that subserve a lasting increase in outflow resistance (4–6). TM cells express major histocompatibility complex proteins and Toll-like receptor 4 receptors (TLR4) and help maintain the immune privilege in the anterior eye *via* phagocytosis and TGFβ2 signaling (7). TLR4 expression is increased in glaucoma, TGFβ-TLR4 crosstalk is involved in production of ECM and regulation of IOP, whereas a mutation in TLR4 inhibited TGFβ2-induced ocular hypertension in mice (7). These observations suggest that the innate immune system might be involved in pressure-dependent differentiation of TM cells into profibrogenic myofibroblasts (8) yet the molecular mechanisms that underlie pressure-dependent TRL4 activation, TGFβ signaling and ECM remodeling remain unknown. Recent studies showed that TM cells sense acute and chronic mechanical stressors *via* arrays of mechanosensitive proteins that include integrins, the cytoskeleton, and stretch-activated ion channels (SACs) (9–11) such as TRPV4. This nonselective cation channel responds to TM substrate deformation with Ca^{2+} influx that regulates cytoskeletal and lipid dynamics, Rho signaling and cell-ECM interactions to facilitate myofibroblast differentiation (12–14). Excessive TRPV4 activity was suggested to drive the pressure-induced increase in TM stiffness and contractility (5, 14, 15) but it is not known how the channel responds to sustained activation.

The human TRPV4 gene contains 16 exons that encode a protein consisting of a proline-rich (PRD) domain, phosphoinositide binding site, ankyrin repeats and a helix-turn-helix (HTH) linker domain within the N-terminus, six transmembrane domains with the pore between S5-S6, and modulatory sites (TRP domain, MAP7-binding domain, CaM/IP3R-binding domain, PDZ domain) in the C-terminus that endow the channel with sensitivity to temperature, metabolites of arachidonic acid, nociceptive and mechanical stimuli (16, 17). Gain- and loss-of-function mutations in the TRPV4 gene cause debilitating skeletal abnormalities, sensorimotor neuropathies and vision loss (18), indicating that the channel is required for homeostatic transduction of sensory information. TRPV4 overactivation and exposure to TGFβ induce transdifferentiation of epithelial, endothelial, and smooth muscle cells into hypersecretory and contractile myofibroblasts (19, 20). Interactions with a wide array of proteins (aquaporins, BK channels, kinases, actin) and processes (Ca^{2+} release from intracellular stores, receptor-operated and store-operated Ca^{2+} influx) (13, 21–24) indicate that TRPV4 exerts its functions within a multiplicity of biological contexts.

The aim of this study was to simulate sustained application of mechanical stress in the absence of confounding effects of the *in situ* milieu and attendant activation of auxiliary stretch-activated channels (SACs) such as TREK-1 and Piezo1 (10, 11). We report that continual chemical stimulation of TRPV4 channels [P_{Ca}/P_{Na} = 10 (25)] induces $[Ca^{2+}]_i$ fluctuations that require TRPM4, a Ca^{2+}-activated monovalent cation channel [P_{Ca}/P_{Na} = 0.12 (26)] that has been linked to hypertension and Ca^{2+} oscillations and Ca^{2+} release from intracellular compartments in lymphocytes and macrophages (27–30). TRPV4 and TRPM4 were also implicated in the maturation of phagocytic function, with disruption of either TRPV4 or TRPM4 signaling in monocytes and macrophages resulting in profound dysregulation of Ca^{2+} homeostasis, LPS-stimulated phagocytosis and survival (31, 32). These findings identify a mechanism that couples TM mechanosensing to endogenous oscillatory activity, with potential functions in innate immune regulation and outflow resistance in the anterior eye.

MATERIALS AND METHODS

Primary Cell Isolation and Culture

Primary trabecular meshwork cells (pTM) were isolated from juxtacanalicular and corneoscleral regions of the human donors' eyes (56 years-old male, 62 years-old female) with no recorded history of eye disease as described (10, 11, 13). The tissues were obtained through the Lions Eye Bank at the Moran Eye Center at the University of Utah and were used in concordance with the tenets of the WMA Declaration of Helsinki and the Department of Health and Human Services Belmont Report. A subset of biochemical experiments was conducted in parallel with immortalized cells (hTM), isolated from the juxtacanalicular region of the human eye (ScienCell Research Laboratories, Carlsbad, CA, USA). The cell phenotype was periodically profiled for expression of *MYOC, TIMP3, AQP1, MGP, ACTA2* (α-smooth muscle actin, αSMA) genes and DEX-induced upregulation of myocilin protein (11, 14).

Passage 2 – 6 cells were seeded onto Collagen I-coated coverslips and grown in Trabecular Meshwork Cell Medium (ScienCell, Catalog#6591; Carlsbad, CA, USA) supplemented with 2% fetal bovine serum (FBS), 100 units/ml penicillin, 100 ug/ml streptomycin, at 37°C and pH 7.4. Cells were transfected with scrambled shRNA (Sc-shRNA) or *Trpm4* shRNA using Lipofectamin™ 3000 (5 μg per 25 cm^2 tissue culture flask). shRNA -transfected cells were identified by green (GFP) or red (mCherry) fluorescence. Knockdown efficiency of TRPM4 shRNA was validated in HEK 293T cells overexpressing GFP-hTRPM4, scrambled shRNA or one of three *TRPM4* shRNA constructs. shRNA1 and shRNA2, with target sequences GGACATTGCCCAGAGTGAACT (1218–1238) and GGAAAGACCTGGCGTTCAAGT (1835–1855), showed >65% knockdown efficiency (**Supplementary Figure 1**). Experiments were conducted 3 - 4 days post- transfection.

Reagents

GSK1016790A (GSK101) is a highly specific agonist (16, 17, 23) and HC067047 (HC-06) antagonist, of TRPV4 channels. Both were

purchased from Sigma (St. Louis, MO) or Cayman Chemical (Ann Arbor, MI). Salts were purchased from Sigma (St. Louis, MO) or VWR (Radnor, PA), CBA (4-chloro-2-[[2-(2-chlorophenoxy) acetyl aminobenzoic acid from Tocris Bioscience (Minneapolis, MN), and BAPTA (1,2-Bis(2-aminophenoxy)ethane-N,N,N',N'-tetraacetic acid) from Alfa Aesar (Tewksbury, MA). The TRPM4 antagonist 9-phenanthrol (9-PA) was from Tocris Bioscience (Bristol, UK). GSK101 (1 mM), and HC-06 (20 mM) DMSO stocks were diluted in extracellular saline (98.5 mM NaCl, 5 mM KCl, 3 mM $MgCl_2$, 2 mM $CaCl_2$, 10 mM HEPES, 10 mM D-glucose, 93 mM mannitol), with final DMSO concentration not exceeding 0.1%.

Immunocytochemistry

Cells

Cells were plated on collagen Type 1-coated glass cover slip 1 day prior to fixation with the 4% PFA for 10 minutes at RT. The samples were blocked with phosphate-buffered saline containing 0.3% Triton X-100 and 5% FBS for 30 minutes at a room temperature (RT). The primary polyclonal rabbit antibody was diluted 1:1000 in PBS (2% BSA and 0.2% Triton X-100) and incubated overnight at 4°C (32). After rinsing, cells were incubated for 1 hour at RT with goat anti-mouse and goat anti-rabbit IgG (H + L) secondary antibodies conjugated to fluorophores (Alexa Fluor 488 nm, 568 nm and/or 594 nm; 1:500; Life Technologies, Carlsbad, CA, USA). Unbound antibody was rinsed, and conjugated fluorophores protected with Fluoromount-G (Southern Biotech, Birmingham, AL, USA) prior to mounting coverslips. Images were acquired on a confocal microscope (FV1200; Olympus, Center Valley, PA) at 1024 x 1024 pixels with a 20x water superobjective (1.00 N.A.; field size: 158.565 x 158.565 μm; 0.155 μm/pixel; sampling speed: 10.0 us/pixel; 12 bits/pixel). ≥50 cells per experiment were acquired for at least 4 independent experiments (n ≥ 200 in total; N ≥ 4).

Tissue Immunohistochemistry

Anterior chambers were fixed in 4% paraformaldehyde for 1 hour, cryoprotected in 15 and 30% sucrose gradients, embedded in Tissue-Tek® O.C.T. (Sakura, 4583), and cryosectioned at 12 μm, as described (13, 30). Sections were probed with a polyclonal rabbit TRPM4 antibody (1:100 (32); and aquaporin-1 mouse monoclonal antibody (1:1000; Santa Cruz Biotechnology Sc-25287). Secondary antibodies were anti-rabbit IgG DyLight 488 (Invitrogen, 35552) and anti-mouse IgG DyLight 594 (Invitrogen, 35511). Sections were coverslipped with DAPI-Fluoromount-G (Electron Microscopy Sciences, Hatfield, PA, 17984-24) and imaged with a confocal microscope. Images were acquired using identical (HV, gain, offset) parameters.

Semiquantitative Real Time-PCR

Total RNA was extracted using Arcturus PicoPure RNA Isolation Kit (ThermoFisher, Cat. No.: KIT0204) (33, 34). 100 ng of total RNA was used for reverse transcription. First-strand cDNA synthesis and PCR amplification of cDNA were performed using qScript™ XLT cDNA Supermix (Quanta Biosciences, Cat. No. 95161). The samples were run on 2% agarose gels using ethidium bromide staining along with the 100-bp DNA ladder (ThermoFisher Scientific, Waltham, MA, Cat. No.: S0323). The primers used in the study are listed in **Table 1**.

Western Blot

TM cells were detached from culture flasks by trypsinization and centrifuged at 2000 rpm for 3 minutes. The cell pellet was washed with PBS and lysed in a RIPA Buffer System (Santa Cruz Biotechnology, Dallas, TX). Cell lysates were separated by 10% SDS-PAGE followed by electrophoretic transfer to polyvinylidene difluoride membranes (Bio-Rad, Hercules CA). Membranes were blocked with 5% skim milk in PBS containing 0.1% Tween 20 and incubated at 4°C overnight with the TRPM4 antibody, following by 3 washes with PBS containing 0.1% Tween-20, blotted with HRP-conjugated GAPDH antibody for 30 min at room temperature and washed with PBS containing 0.1% Tween 20. The signals were visualized with an enhanced chemiluminescence system (FluorChem Q, Cell Biosciences, Santa Clara, CA).

Ion Imaging

Pharmacological experiments were conducted on a microscope stage in a fast-flow chamber (RC26GLP, Warner Instruments, Hamden CT) connected to a gravity-fed perfusion system. The flow rate of the solution was regulated *via* individual pinch valves (VC-6; Warner Instruments; Holliston, MA). Primary cells were loaded with Fura-2 AM (3 μM; Invitrogen/ThermoFisher Scientific) for 45 min at RT. The cells were perfused with extracellular solution containing (mM): 135 NaCl, 2.5 KCl, 1.5 $MgCl_2$, 1.8 $CaCl_2$, 10 HEPES, 5.6 D-glucose (pH = 7.4, osmolarity = 300 - 303 mOsm). Epifluorescence imaging was performed on Nikon microscopes using 40x (1.3 N.A., oil or 0.80 N.A., water) objectives, 340 nm and 380 nm excitation filters (Semrock, Lake Forest, IL, USA) and a Xenon arc lamp (DG4, Sutter Instruments). Fluorescence emission at 510 nm, in response to alternating 340/340 excitation, was captured with cooled

TABLE 1 | Primer sequences used for PCR analysis.

Name	Forward primer	Reverse primer	Product size (bp)	NCBI reference number
TRPM4	GATGCACACCACGGAGAA	AGAGCCGGAGGAAATTGCTG	91	NM_017636.4
TRPV1	GCCCAGCATGTTCCCAAATC	TGTCCCAGTAGAGACTGACCA	169	NM_080704.3
TRPV4	TCCCATTCTTGCTGACCCAC	AGGGCTGTCTGACCTCGATA	217	NM_021625.4
MYOC	CCACGTGGAGAATCGACACA	TCCAGTGGCCTAGGCAGTAT	118	NM_000261.1
AQP1	TGGAGCAAGCTCTTCCCTTG	CTGTCCTTGGGCTGCAACTA	174	NM_198098.3
GAPDH	CTCCTGTTCGACAGTCAGCC	GACTCCGACCTTCACCTTCC	89	NM_002046.5

EMCCD or CMOS cameras (Photometrics, Tucson, AZ). Data acquisition was controlled by NIS Elements 3.22 software (Nikon). Typically, ~5-10 cells per slide were averaged across ~3-6 slides per experiments, with at least 3 independent experiments ($n \geq 50$; $N \geq 3$). The experiments were performed at room temperature (20 - 22°C).

Ca^{2+} imaging. Cells were loaded with 3 μM Fura-2 AM (Invitrogen/ThermoFisher) (K_d at RT = 225 nM) for 45 min. ΔR/R (peak F_{340}/F_{380} ratio – baseline/baseline) was used to quantify the amplitude of Ca^{2+} signals (e.g (13, 35). Only transient Ca^{2+} events with amplitudes exceeding three standard deviations of baseline fluctuations were included in analysis.

Intracellular Na^+ imaging. Cells were loaded with 3 μM NaTRIUM Green™-2 AM (TEFLabs Austin, TX) for 50 – 60 min in a cell culture incubator at 37°C. Fluorescence was acquired at 484 nm excitation and 520 nm emission (Semrock, Rochester, NY). Na^+ signals were normalized to the average baseline (F/F_o) obtained at the beginning of the experiments.

Electrophysiology

Whole cell and single-channel techniques were used to record membrane currents (voltage clamp) or voltage (current clamp) (11, 35, 36). Borosilicate patch pipettes (WPI, Sarasota, FL) were pulled to resistances of 5 - 8 MΩ (P-2000; Sutter Instruments, Novato CA). The standard pipette solution contained (in mM): 125 NaCl, 10 KCl, 10 HEPES, 1 $MgCl_2$, 2 ethylene glycol-bis(β-aminoethyl ether)-N,N,N',N"-tetraacetic acid (EGTA), 0.3 Na-GTP (pH 7.3) The pipette solution for recording Ca^{2+}-activated current contained (in mM): 125 Na-gluconate, 10 HEPES, 1 $MgCl_2$, 0.01 $CaCl_2$, 0.3 Na-GTP (pH 7.3). Nominally Ca^{2+}-free pipette solution (standard) contained (in mM): 125 Na-gluconate, 10 HEPES, 1 $MgCl_2$, 5 BAPTA, 0.3 Na-GTP (pH 7.3). The standard extracellular solution contained (in mM): 135 NaCl, 2.5 KCl, 1.5 $MgCl_2$, 1.8 $CaCl_2$, 10 HEPES, 5 D-glucose (pH 7.4). The extracellular solution for recording Ca^{2+}-activated current contained (in mM): 135 Na-gluconate, 10 HEPES, 1 $MgCl_2$, 1.8 $CaCl_2$, 0.3 Na-GTP (pH 7.3). The bathing solution for excised (inside-out) patch clamp experiments contained (mM): 140 NaCl, 2.5 KCl, 1.5 $MgCl_2$, 1.8 Ca^{2+} or 10 EGTA, 5.6 D-glucose, 10 HEPES (pH 7.4, adjusted with NaOH). The pipette solution used in excised patch recordings contained 140 NaCl, 2.5 KCl, 1.5 $MgCl_2$, 1.8 $CaCl_2$, 5.6 D-glucose, 10 HEPES (pH 7.4, adjusted with NaOH). Experiments were performed at room temperature of 21-22°C.

Patch clamp data in whole-cell and single-channel configurations was acquired with a Multiclamp 700B amplifier and a Digidata 1550 interface, and controlled by Clampex 10.7 (Molecular Devices, Union City, CA). Cells were held at -100 mV or +100 mV, with currents sampled at 5 kHz, filtered at 2 kHz with an 8-pole Bessel filter and analyzed with Clampfit 10.7 (Molecular Devices) and Origin 8 Pro (Origin Lab, Northampton, MA). Whole-cell currents were elicited by voltage ramps ascending from -100 mV to 100 mV (0.2 V/sec) from the holding potential of 0 mV. The time course of Ca^{2+}-activated currents was obtained by subtracting voltage ramp-evoked currents traces recorded 40 s after obtaining the whole-cell configuration from preceding and following traces. I-V curves of Ca^{2+}-activated currents were assessed by subtracting currents recorded 40 s after obtaining the whole-cell configuration from steady state currents recorded 4 min after obtaining the whole-cell configuration.

Patch clamp combined with fluorescent imaging. Cells were loaded with a calcium indicator Fluo-4 (Invitrogen/ThermoFisher) through a patch pipette. Fluorescence signals in voltage-clamped cells were detected using the excitation filter 484 nm and the emission filter 520 nm (Semrock, Lake Forest, IL). VOCC-mediated current was recorded in the extracellular solution containing as following (mM): 115 NaCl, 2.5 KCl, 20 $BaCl_2$, 1.5 $MgCl_2$, 10 HEPES, 5.6 D-glucose.

Outflow Facility Measurement: iPerfusion

Procedures on living mice were carried out under the authority of a UK Home Office project license and adhered to the ARVO Statement for the Use of Animals in Ophthalmic and Vision Research. The outflow facility in enucleated eyes from C57BL/6J mice (N = 5 mice; 11-week-old males; Charles River UK Ltd., Margate, UK) was measured using *iPerfusion*, a custom-made microfluidic setup (37, 38). Following cervical dislocation, eyes were enucleated and affixed to a support platform using tissue glue. Eyes were submerged in a PBS bath kept at 35°C throughout the perfusion. Using a micro-manipulator under a dissection microscope, the anterior chamber was cannulated within 10 minutes of death using a glass micropipette pulled to have a 100 μm diameter beveled tip. The perfusion fluid was Dulbecco's PBS containing divalent cations and 5.5 mM glucose (DBG) that was sterile filtered (0.25 μm) prior to use.

One eye was perfused with 9-PA (25 μM) whilst the contralateral eye was perfused with vehicle (perfusion fluid containing the same concentration of DMSO). IOP was set to 9 mmHg for 1 hour to pressurize and acclimatize the eye to the perfusion environment and to allow sufficient time for 9-PA to reach the outflow tissues. Flow into the eye was then measured over 8 increasing pressure steps from 6.5 to 17 mmHg. Steady state for each step was evaluated when the ratio of the flow rate to pressure changed by less than 0.1 nl/min/mmHg per minute over a 5-minute window (37). The stable pressure, P, and flow rate, Q, were calculated over the last 4 minutes of each step, and a power-law relationship of the form

$$Q = C_r \left(\frac{P}{P_r}\right)^{\beta} P \quad \text{Eq. 1}$$

was fit to the $Q - P$ data. The reference outflow facility, C_r, represents the value of outflow facility at a reference pressure P_r of 8 mmHg, and β characterizes the non-linearity of the Q-P relationship (37). The relative difference in C_r between treated and untreated contralateral eyes was then calculated as the ratio of C_r in the treated eye relative to that in the contralateral control eye minus unity. We evaluated whether the relative difference in facility was statistically different from zero using a weighted t-test on the log-transformed data, as previously described (37). Facility values and relative changes in facility are reported in terms of the geometric mean and the 95% confidence interval on the mean.

IOP Measurement

Male and female C57BL/6J mice (JAX; Bar Harbor, ME) and homozygous pan-TRPM4 KO mice (39) were maintained in a pathogen-free facility with a 12-hour light/dark cycle and *ad libitum* access to food and water. The experimental protocol was approved by the animal ethics committee at the University of Utah and adhered to the tenets of the ARVO Statement for the Use of Animals in Ophthalmic and Vision Research. No sex differences were noted in the data, which were pooled. A TonoLab rebound tonometer was used to measure IOP in mice between noon and 2 PM, as described (13). In animals habituated to handling for several days preceding the IOP measurement. An IOP reading represents an average of 10 to 20 tonometer readings.

Statistical Analysis

Student's paired t-test or two-sample t-test (OriginPro 9.0; OriginLab, Northampton, MA) were applied to estimate statistical significance of results. $P < 0.05$ was considered statistically significant. Results are presented as the means ± S.E.M. A preprint of this article was submitted at https://biorxiv.org/cgi/content/short/2021.12.15.472700v1.

RESULTS

Activation of TRPV4 Induces Fluctuations of $[Ca^{2+}]_i$

Unstimulated TM cells from healthy donors have low basal $[Ca^{2+}]_i$ and rarely show Ca^{2+} fluctuations (13) but previous studies of mechanically evoked Ca^{2+} signaling in TM cells have been limited to short stimulation paradigms (5-10 min) (11, 13) and little is known about how the TM regulates $[Ca^{2+}]_i$ in the presence of sustained TRPV4 activity. To investigate the mechanisms that underlie Ca^{2+} signaling downstream from the channel, Fura-2-loaded human TM cells were stimulated for 30 – 45 min with bath-applied agonist GSK101 (25 nM). Agonist-evoked $[Ca^{2+}]_i$ increases peaked within 2-3 min, followed by a gradual decline to a steady plateau at ~27% of the peak (**Figures 1**, **2**). A subset (~50%) of cells showed an increase in the frequency of Ca^{2+} fluctuations during the plateau phase whereas cells treated with the TRPV4 antagonist HC067047 (HC-06; 5 μM) (**Figures 1B, C**), broad-spectrum inhibitors of TRP channels such as Ruthenium Red, or Ca^{2+} -free saline (**Figure 2**), did not exhibit this time-dependent behavior.

Oscillatory Ca^{2+} signals can reflect activation of voltage-operated mechanisms within the membrane and/or release from internal compartments. Voltage-dependent mechanisms were tested by stimulating the cells in the current-clamp mode. The agonist evoked a ~15 mV shift in the membrane potential (**Figures 3A, C**) that was maintained over the course of the experiment (e.g., 40 min after agonist application; red trace in **Figure 3B**) and was not associated with changes in temporal behavior.

L-type voltage-operated Ca^{2+} channels have been implicated in calcium oscillations and pressure-dependent contractility in smooth muscle cells (40). To test their involvement, we combined imaging in Fluo-4-loaded cells with whole-cell recording. As shown in **Figure 3D**, stepping the holding potential from the holding potential of -70 mV to 0 mV had no detectable effect on the Ca^{2+} signal. Similarly, extracellular $BaCl_2$ (20 mM) which permeates voltage-operated Ca^{2+} channels without inactivating the channel pore or stimulating Ca^{2+} release from ER stores (41–43) did not induce depolarization-evoked inward currents or Ca^{2+} spiking (**Figure 3Ei**) whereas retinal ganglion cells responded with an inward current (**Figures 3Eii, F**) that was blocked by the L-type channel blocker nimodipine (1 μM) (**Figure 3Fii**). These data suggest that TRPV4-dependent Ca^{2+} oscillations in human TM cells do not involve L-type voltage-operated Ca^{2+} channels activity.

TRPV4-Induced Ca^{2+} Fluctuations Require TRPM4

To further investigate the mechanism that underlies TRPV4-induced calcium oscillations, cells were loaded with the Na^+-sensitive indicator NaTRIUM Green-2 and exposed to GSK101. The agonist stimulated an increase in $[Na^+]_i$ in 54% (39/73) cells (5.96 ± 0.81% above baseline; $p < 0.0001$; $n = 39$). The increase in Na^+ concentration was not associated with an oscillatory component, indicating that TRPV4-induced Na^+ influx is distinct from mechanisms that subserve Ca^{2+} oscillations. We tested the potential involvement TRPM4, a Ca^{2+}-activated channel permeable to monovalent ions that has been implicated in $[Ca^{2+}]_i$ oscillations in T cells, cardiomyocytes, and smooth muscle cells (27, 28, 40) but with no known functions in the eye by exposing the cells to GSK101 in the presence of 9-phenanthrol (9-PA, 40 μM), an intracellularly acting benzoquinolizinium inhibitor of the channel (44, 45). 9-PA reversibly attenuated the increase in $[Na^+]_i$ evoked by GSK101 ($P < 0.001$) (**Figures 4A, B**), and obliterated Ca^{2+} fluctuations during the plateau response phase (**Figures 4C, D**) ($P < 0.0001$).

Histology: TM Cells Express TRPM4

Transcriptional profiling of immortalized (hTM) and primary (pTM) cells showed robust expression of TRPM4 and TRPV4 transcripts (**Figure 5A**) together with TM markers myocilin and aquaporin 1, at bp sizes that matched expected sizes for their respective DNAs. The overall levels of TRPM4 transcripts in hTM cells were comparable to TRPV4 mRNA, and ~35% of TRPV4 mRNA in primary cells (**Figure 5B**). In both cell lines, a validated antibody (32) labeled a Western blot band at ~130 kDa (**Figure 5C**), corresponding to the known M.W. of the TRPM4b protein variant (46). Confocal examination of TRPV4-immunol reactive cells and intact tissue further showed labeling of the plasma membrane and cytosolic puncta (**Figure 5Dii**) and cytosolic puncta. In the preparation from the mouse anterior eye, TRPM4-ir was distributed across the juxtacanalicular and corneoscleral TM regions (green), where it colocalized with the TM marker Collagen IV. Additional, albeit more modest, TRPM4-ir signals were also detected in the ciliary body and the retina.

Electrophysiology: TM Cells Functionally Express TRPM4

We next assessed the properties of the TRPM4-mediated current in voltage-clamped cells by probing for a Ca^{2+}-sensitive monovalent

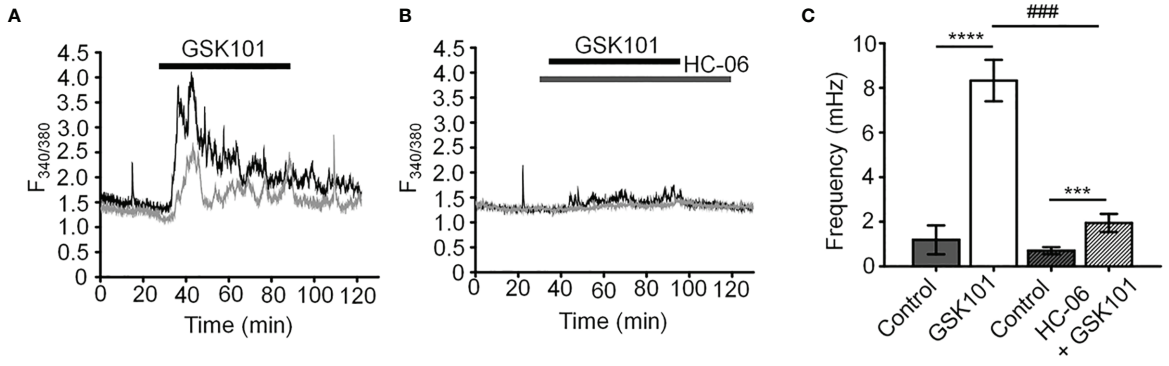


FIGURE 1 | GSK101 triggers intracellular Ca^{2+} oscillations in hTM cells. **(A)** Representative traces of $[Ca^{2+}]_i$ oscillations in GSK101 treated TM cells. **(B)** GSK101-induced oscillations are absent in cells pretreated with HC-06. **(C)** Quantification of results shown in **(A, B)**, shown as average ± S.E.M. ****P < 0.0001, ***P < 0.001 (paired-sample t-test), ###P < 0.001 (two-sample t-test), n = 49 cells and n = 38 cells for control/GSK101 and control/HC06+GSK101 groups, respectively.

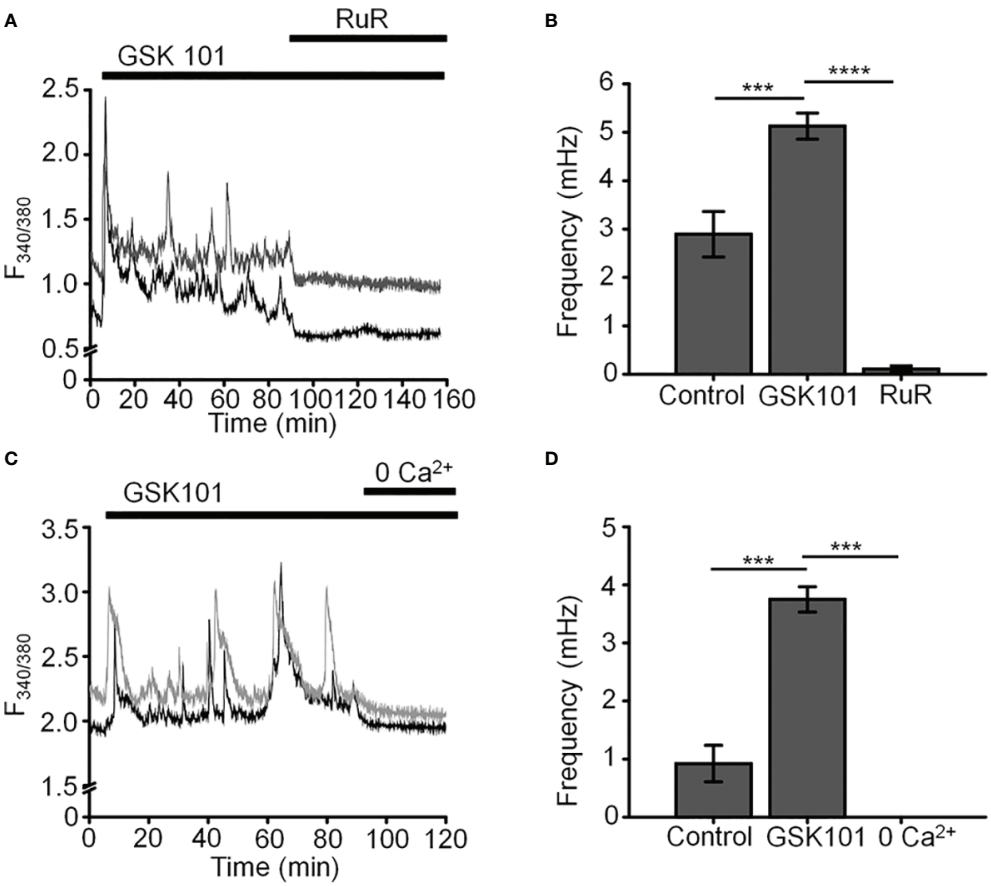


FIGURE 2 | GSK101-induced $[Ca^{2+}]_i$ oscillations requires activity of Ca^{2+} -permeable and Ca^{2+} -dependent TRP channels. Shown are representative traces. **(A, C)** GSK101-induced $[Ca^{2+}]_i$ fluctuations are abolished by the nonselective TRP blocker Ruthenium Red (RuR; 10 μM) and in the absence of free extracellular Ca^{2+}. **(B, D)** RuR and Ca^{2+}-free solution abolish GSK101 induced $[Ca^{2+}]_i$ oscillations. Mean ± S.E.M. ***P < 0.001, ****P < 0.0001, paired t-test, n = 51 and n = 43 cells for **(B, D)**, respectively.

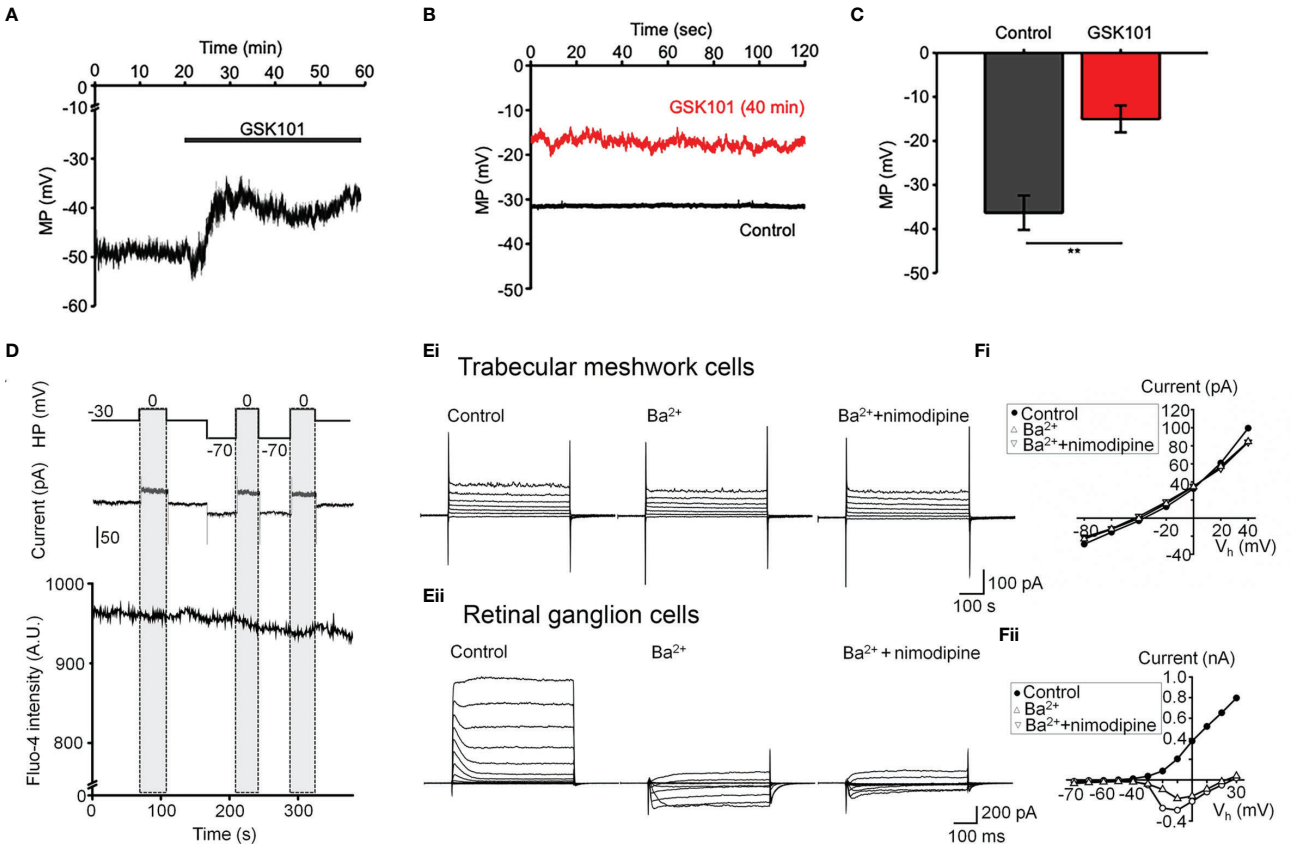


FIGURE 3 | GSK101 depolarizes TM cells, but they lack functional L-type voltage-operated Ca^{2+} channels **(A–C)** Current clamp. GSK101 depolarizes the cells, with the effect maintained over 40 min (red trace vs. black trace denoting the unstimulated control in B). **(D)** Combined whole cell recording and calcium imaging. The voltage protocol (upper trace), depolarization-evoked whole-cell current (middle trace), time-lapse of Fluo-4 fluorescence (lower trace). Shadowed bars indicate the depolarizing steps. **(E, F)** Representative whole-cell currents elicited by voltage steps in TM cells (Ei; n = 15) **(B)** and mouse retinal ganglion cells (Eii; n = 5), respectively. **(F)** Voltage-current relationships derived from cells shown in **(E)**. The current was measured at the end of each voltage pulse.

current (47, 48). Cells were dialyzed with pipette solutions containing 10 μM or zero Ca^{2+} and Ca^{2+}-activated K^+ and Cl^- conductances were minimized by replacing extra/intracellular K^+ ions (with Na^+) and Cl^- ions with gluconate (47). ~50% of cells dialyzed with the Ca^{2+}-containing solution showed time-dependent increases in inward and outward whole-cell currents. The current-voltage relationship of the Ca^{2+}-dependent current showed modest outward rectification and peaked within ~4 min after obtaining the whole-cell configuration (**Figure 6A**), had a reversal potential of 1.6 ± 2.9 mV and amplitudes of -122.7 ± 61.5 pA and 211.2 ± 93.7 pA at holding potentials of -100 mV and 100 mV, respectively, (**Figure 6B**). The current was inhibited by 9-PA (20 μM; n=7/7) and was not observed in cells dialyzed with Ca^{2+}-free solutions or exposed to bath-applied Ruthenium Red (10 μM) (n = 5/5) (**Figure 6A**).

Single channel properties of the Ca^{2+}-activated current were additionally investigated in inside-out membrane patches using symmetrical Na^+ gluconate-based pipette and extracellular solutions. Patch excision in 1.8 mM Ca^{2+}-containing saline triggered a rapidly inactivating channel with a linear current-voltage relationship (n = 15/85 patches; **Figures 6C, F**). The slope conductance of the unitary current was 18.9 ± 0.6 pS and the amplitude at 100 mV was 2.05 ± 0.04 pA (**Figures 6D–F**). The channel was facilitated at positive membrane potentials, inhibited by 9-PA (**Figures 6C, D**), and typically inactivated within ~5 min after patch excision. Its activity was abolished in Ca^{2+}-free saline (**Figure 6C**). Both whole-cell and single channel properties of the Ca^{2+}-induced current in TM cells are consistent with TRPM4 activity.

TRPM4 Is Required for TRPV4-Dependent Ca^{2+} Oscillations

To more specifically test the role of TRPM4 in $[Ca^{2+}]_i$ fluctuations, we transfected the cells with TRPM4-specific short-hairpin (shTRPM4-GFP) or "scrambled" (Sc-GFP) control shRNAs (**Figure 7A**). Of the 3 TRPM4-shRNA constructs, we utilized Sh#1 which downregulated TRPM4 mRNA by 80% (**Supplementary Figure 1**). Compared to Sc-shRNA-expressing controls, TRPM4 shRNA-transfected cells showed ~80% reduction in the frequency of TRPV4-induced Ca^{2+} fluctuations (**Figures 7B–D**).

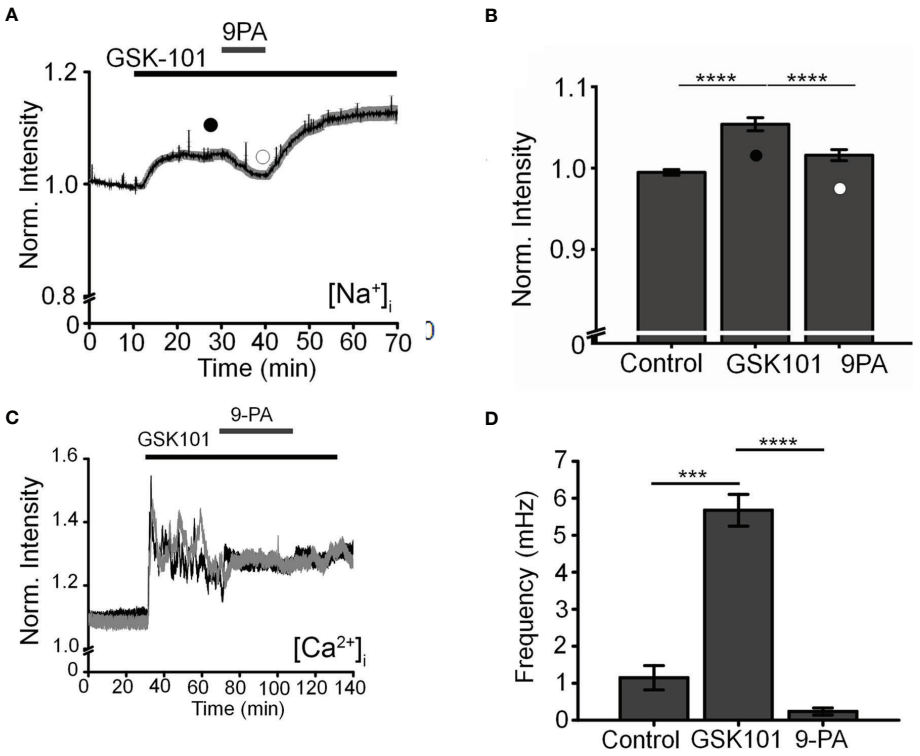


FIGURE 4 | TRPM4 mediates TRPV4-induced Na^+ influx and facilitates Ca^{2+} fluctuations. **(A).** Averaged time lapse ratio in NaTRIUM Green-loaded TM cells. GSK101-evoked increase in $[Na^+]_i$ is partially and reversibly suppressed by 9-PA. **(B)** Mean ± S.E.M. values for the experiment in A (n = 10). Black and white symbols represent time at which the intensity was measured. **(C)** GSK101-evoked $[Ca^{2+}]_i$ oscillations are suppressed by 9-PA (n = 39). **(D)** Summary of the data shown in **(C)**, as mean ± S.E.M. *** = P < 0.001, **** = p < 0.0001, paired-sample t-test.

We also tested the TRPM4-dependence of TRPV4-induced calcium signals by transfecting HEK293 cells with TRPV4 and/or TRPM4 DNA. TRPV4 only-transfected cells responded to GSK101 with a peak $[Ca^{2+}]_i$ increase that inactivated to a plateau without showing time-dependent Ca^{2+} oscillations whereas cells co-transfected with TRPV4 + TRPM4 DNA displayed robust oscillations in the presence of GSK101 (**Supplementary Figure 2**).

TRPM4 Does Not Regulate Trabecular Outflow or Steady-State Intraocular Pressure

Chronic TRPV4 activation was suggested to suppress aqueous humor drainage in hypertensive mouse eyes (13). Given that 9-PA inhibits TRPV4-dependent Ca^{2+} oscillations *in vitro* (**Figures 8A, B**), we tested whether it influences the trabecular component of pressure-induced fluid outflow ("outflow facility"). The effect of 9-PA on outflow facility was examined in enucleated mouse eyes using the *iPerfusion* system (37, 38). In response to 25 μM 9-PA, outflow facility decreased by -5% [-23%, 18%] (geometric mean [95% CI]; **Figure 8A**) relative to contralateral eyes that were perfused with vehicle, but this difference was not statistically significant (p=0.38, n=5 pairs). C_r for 9-PA treated eyes was 5.4 [4.2, 6.9] nl/min/mmHg and 5.5 [4.6, 6.7] nl/min/mmHg for vehicle-treated eyes (**Figure 8A**).

Finally, we investigated whether genetic deletion of TRPM4 channels affects intraocular pressure homeostasis in the mouse eye. $TRPM4^{-/-}$ eyes showed intraocular pressure levels (11.86 ± 0.14 mm Hg that were comparable to controls (12.10 ± 0.16 mm Hg; p > 0.05; n = 14 eyes and n = 36 eyes for WT and $TRPM4^{-/-}$, respectively), indicating that TRPM4 may not be required for steady-state intraocular pressure regulation **(Figure 8C)**. Overall, these results suggest that TRPM4 signaling is not required for step-induced fluid drainage across the or for steady-state intraocular pressure regulation.

DISCUSSION

The goal of this study was to define the properties of calcium homeostasis during sustained stimulation of TRPV4, a transducer of mechanical stimuli that has been implicated in the regulation of conventional outflow and intraocular pressure (13). We show that long-term TRPV4 stimulation evokes Ca^{2+} oscillations that are independent of the membrane potential and require expression of TRPM4. Both TRPV4 and TRPM4 were strongly expressed in primary and immortalized TM cells, with functional coupling between the two cation channels revealed by the rise of the Ca^{2+}-activated monovalent current and loss of oscillatory response

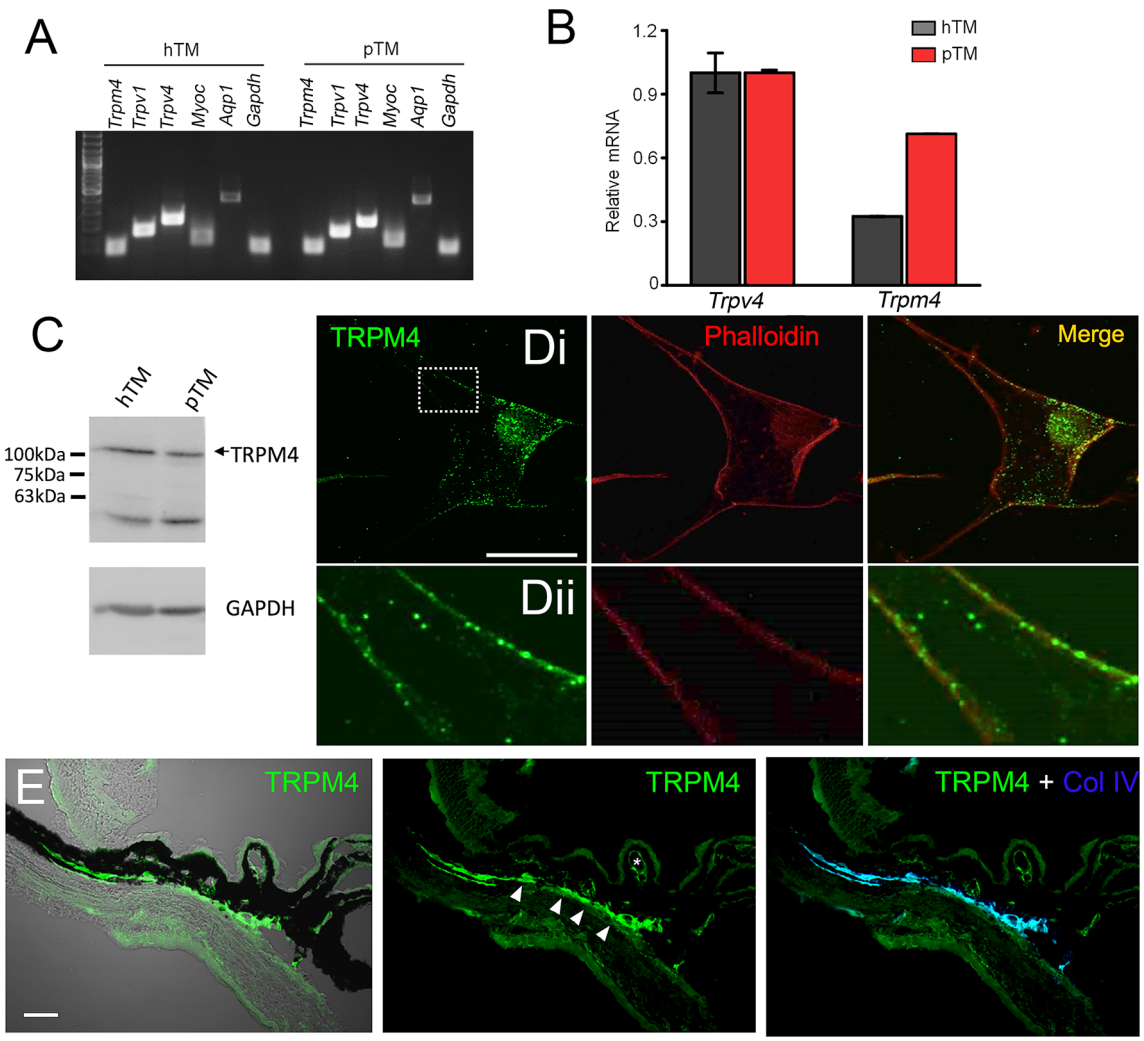


FIGURE 5 | TRPM4 is expressed in TM cells. **(A)** Representative PCR gels show expression of TRPM4 and TRPV4 transcripts together with markers aquaporin 1 (AQP1), TRPV1, and myocilin (MYOC) in immortalized (hTM) and primary (pTM) cells. **(B)** Semiquantitative qRT-PCR. Relative mRNA abundance of TRPM4 vs. TRPV4; expression is normalized to hTM TRPM4; mean ± S.E.M, N = 3. **(C)** Western blot. hTM and pTM cells show a TRPM4 band at the expected M.W. [**(D)**, upper panel] Cultured cells immunolabeled for TRPM4, with a magnified image of the region selected by the square (*inset*) showing punctate signals within the plasma membrane. Scale bar = 50 µm. **(E)** Anterior eye section from a wild type C57 mice, labeled with TRPM4. The TM region shows pronounced TRPM4-ir (arrows) that colocalizes with the marker Collagen IV (Col IV, blue). Moderate signal is seen in the ciliary body (arrows) and ciliary vasculature (asterisk).

following TRPM4 knockdown. Our findings identify novel interactions between TRPV4, TRPM4 and intracellular calcium stores and build a new working model that may help increase our understanding of homeostatic and time-dependent signaling within the primary outflow pathway.

Changes in $[Ca^{2+}]_i$ represent one of the earliest responses of nonexcitable cells to mechanical stress. Resting human TM cells do not exhibit spontaneous calcium activity whereas sustained stimulation of TRPV4 channels produced three types of time-dependent calcium behavior. (i) The initial increase in $[Ca^{2+}]_i$ evoked by GSK101 peaked within 2-4 min and showed slow onset kinetics that was likely shaped by the messenger pathway involving obligatory activation of phospholipase A2 and production of epoxyeicosatrienoic messengers that bind the pocket formed by S2-S3/S4-S5 linker residues (13, 17). (ii) The subsequent relaxation to the steady-state plateau phase reflects Ca^{2+}-dependent channel inactivation, internalization, interactions with modulatory sites within N- and C-termini (16) or negative regulation of Ca^{2+} influx by TRPM4 (44). (iii) The relaxation phase was associated with Ca^{2+} fluctuations in a frequency range similar to signals reported in glaucomatous TM (45) and pressure-, stretch- and GSK101- stimulated fibroblasts and chondrocytes (49, 50).

Several pieces of evidence suggest that the oscillatory response requires TRPM4 signaling. (i) TRPV4-induced fluctuations were suppressed by 9-PA, which also induced a reversible decrease in $[Na^+]_i$; (ii) TRPM4 knockdown in TM cells preserved the GSK101

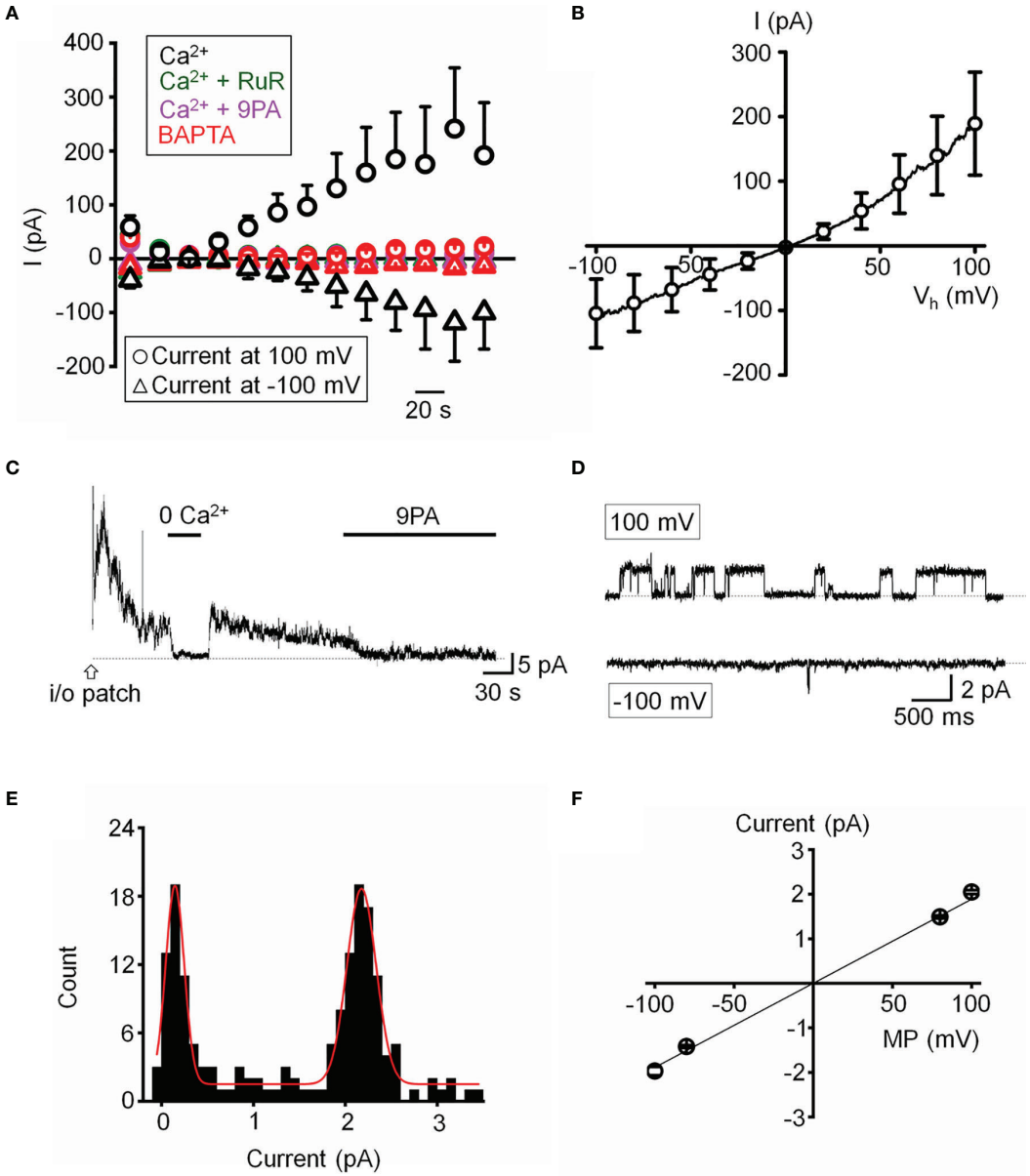


FIGURE 6 | Functional expression of a calcium-activated non-selective cation channels. **(A)** Time course of the whole-cell current recorded at the holding potentials 100 and -100 mV. The pipette solution contained 10 μM Ca^{2+} in the standard saline (*black*, n = 5), with addition of Ruthenium Red (RuR; 10 μM*; olive*, n = 11), 9-PA (20 μM*; magenta*, n = 15) in extracellular solution, or Ca^{2+}-free pipette solution (*red*, n = 15). **(B)** Averaged current-voltage relationship of the Ca^{2+} activated current in A subtracted by the Ca^{2+}-free component (n = 6). **(C)** Representative trace demonstrating the activity of a Ca^{2+}-activated channel in an inside-out patch preparation at +100 mV. **(D)** Representative traces of single channel activity. **(E)** Histogram of unitary current amplitude, fit with Gaussian function (red trace; R-Square = 96.6%). The data were binned at 0.02 pA. **(F)** Current-voltage relationship of single channel current, n = 6 patches. **(A, B, F)** show mean ± S.E.M.

response but eliminated the oscillatory calcium component, and (iii) Heterologous expression of TRPV4 and TRPM4 channels reconstituted fluctuations in HEK293 cells. TRPM4 expression in TM cells was confirmed by transcriptional profiling and immunohistochemistry, with *TRPM4* mRNA levels reaching ~30-70% of *TRPV4* mRNA, and immunoblots showing a band at the predicted M.W. As in other cell types (51, 52), the TRPM4 antibody labeled plasma membrane and intracellular compartments. The former corresponds to full-length TRPM4b variant which forms the Ca^{2+}-activated Ca^{2+}-impermeant cation channel and appears to congregate into punctate clusters within the cell membrane (**Figure 5Dii**) whereas intracellular puncta may correspond to truncated N-terminal variants with unknown functions that localize to the ER (32, 53, 54). The aggregation of TRPM4-ir

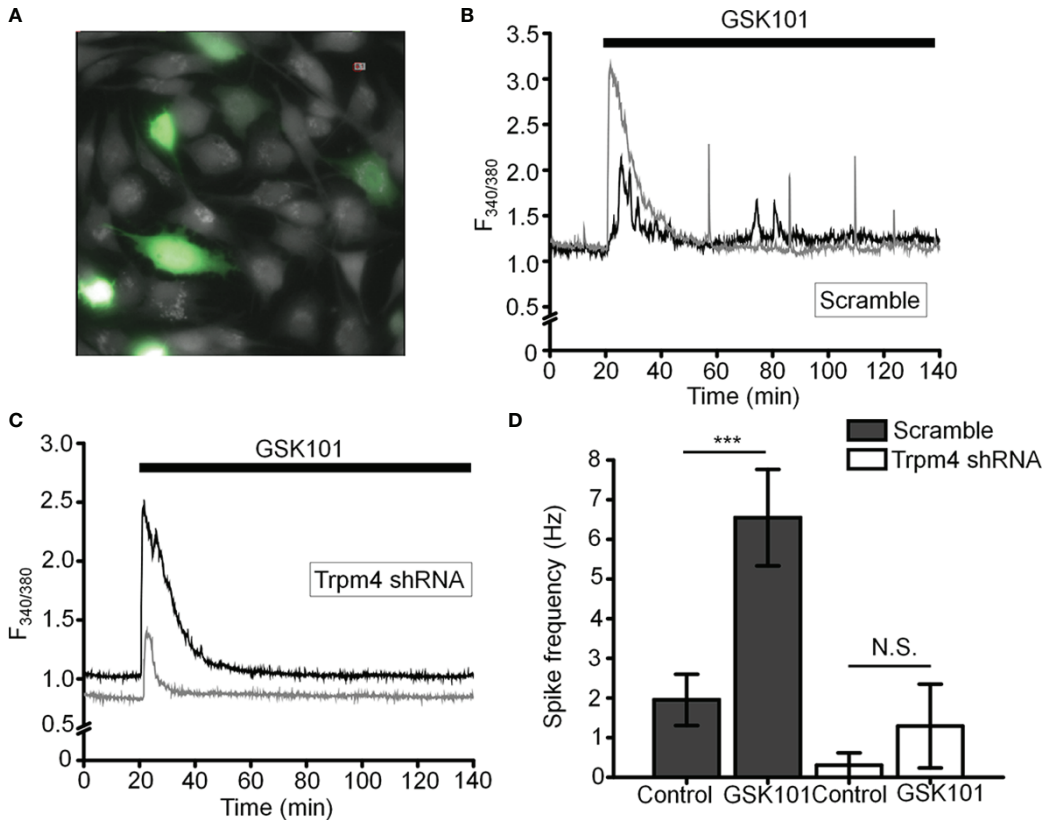


FIGURE 7 | TRPM4 knockdown disrupts GSK101-triggered $[Ca^{2+}]_i$ fluctuations. **(A)** TM cells treated with Sc-GFP, and TRPM4 shRNA-GFP constructs. **(B, D)** Sc-shRNA-transfected cells exhibit fluctuating $[Ca^{2+}]_i$ signals, which show **(C, D)** reduced frequency in TRPM4-shRNA-treated cells. Data shown as mean ± S.E.M. ***P < 0.001, $^{N.S.}$P > 0.05, paired t-test, n = 116 cells and n = 27 cells for Sc- and TRPM4 shRNAs, respectively.

signals resembles mechanosensory clusters enriched in TRPV4, paxillin and pFAK described in TM cells and embryonic fibroblasts (14, 55). Consistent with biochemical analyses, TM cells showed current-voltage relationship and pharmacological profiles characteristic of nonselective calcium-activated monovalent current mediated by TRPM4 (i.e., inhibition by Ruthenium Red, 9-PA and shRNA). Its quasi-linearity points at the membrane presence of PIP2 (56) whereas inhibition by BAPTA indicates that the channel is activated within membrane microdomains within which TRPV4 and TRPM4 functionally interact. Ca^{2+} fluctuations and calcium-activated monovalent current were observed in ~50% of recorded cells, possibly because the cells were derived from multiple TM populations or existed in different stages of the cell cycle. An immortalized atrial cardiomyocyte cell line similarly showed TRPM4-dependent Ca^{2+} oscillations in ~30% cells (28).

The advantage of the synthetic agonist GSK101 was that it allowed us to track signaling mechanisms associated with TRPV4 in the absence of concurrent activation of Piezo1 and TREK-1 stretch-activated channels (e.g (10, 11). In contrast to previous studies in myocytes, smooth muscle cells, neurons and immune cells (27–29, 57) which linked TRPM4-dependent $[Ca^{2+}]_i$ oscillations to obligatory voltage-gated Ca^{2+} influx, TM cells did not show functional voltage-operated calcium channels expression under our experimental conditions. Thus, depolarization had no discernible effect on $[Ca^{2+}]_i$ and the transmembrane current, and Ba^{2+} concentrations that reliably trigger voltage-operated calcium channels-mediated spiking and suppress store release in retinal neurons (15, 41) had no discernable effects on TM signaling. The absence of coupling between the membrane potential, $[Na^+]_i$ and Ca^{2+} oscillations indicates that Ca^{2+} fluctuations reflect intracellular and/or voltage-independent mechanisms. Previous investigation of TRPM4-TRPC3 interactions in HEK293 cells showed that cell depolarization caused by Na^+ influx transiently suppresses TRP-mediated Ca^{2+} influx by reducing the inward electrochemical driving force for Ca^{2+} (48). TRPM4 signaling and oscillations in cardiomyocytes were attributed to redistribution of mitochondrial Ca^{2+} stores into the cytosol (28) but it remains to be determined whether Ca^{2+} transients that underlie the oscillatory response involve ψ_m and mitochondrial transporters (Na^+/Ca^{2+}-Li^+ exchangers, Ca^{2+}/H^+ exchange, and/or MCU uniporters). A simple model delineating the potential players associated with TRPV4-dependent calcium oscillations is shown in **Figure 9**. Another potential source could include reciprocal interactions between Ca^{2+} influx and the IP3R store (55, 55) mediated through contacts between the C-terminus CaM-binding site of TRPV4 and

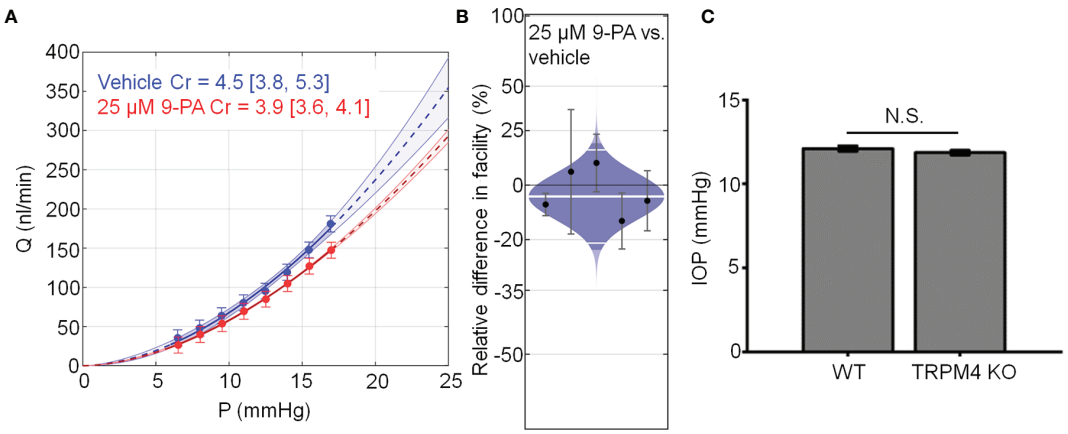


FIGURE 8 | TRPM4 does not regulate trabecular outflow and steady-state intraocular pressure. **(A)** Representative flow-pressure (*Q* – *P*) plot for contralateral eyes perfused with 25 μM 9-PA versus vehicle. Curves show the optimal fit from Equation 1, with 95% confidence bounds and error bars show 95% confidence intervals. **(B)** Relative difference in outflow facility between contralateral eyes perfused with 25 μM 9-PA versus vehicle. The relative difference in facility is defined as the ratio of C_r in the experimental eye perfused with 9-PA relative to vehicle-perfused contralateral eye minus unity, expressed as a percentage. Each data point represents the relative difference in facility for an individual mouse. Error bars are 95% confidence intervals. Shaded regions represent the best estimate of the sample distributions, with the central white line representing the geometric mean. Dark central bands represent the 95% CI on the mean, and the outer white lines represent the limits encompassing 95% of the population. **(C)** Averaged results for intraocular pressure in wild-type (WT, n = 14 eyes) and TRPM4 KO (n = 36 eyes) mice. $^{N.S.}$ = P > 0.05.

the IP3R receptor (58) and depolarization-dependent reduction of the driving force for Ca^{2+} influx through CRAC/Orai channels (27).

TRPM4 was suggested to be directly activated by membrane stretch (59) but this conclusion has been controversial (58, 60, 61). A compelling aspect of our findings is that its role in mechanosignaling might instead reflect activation downstream from stretch-activated channels. Chemical activation of TRPV4 reproduced time-dependent behavior of pressure-induced Ca^{2+}

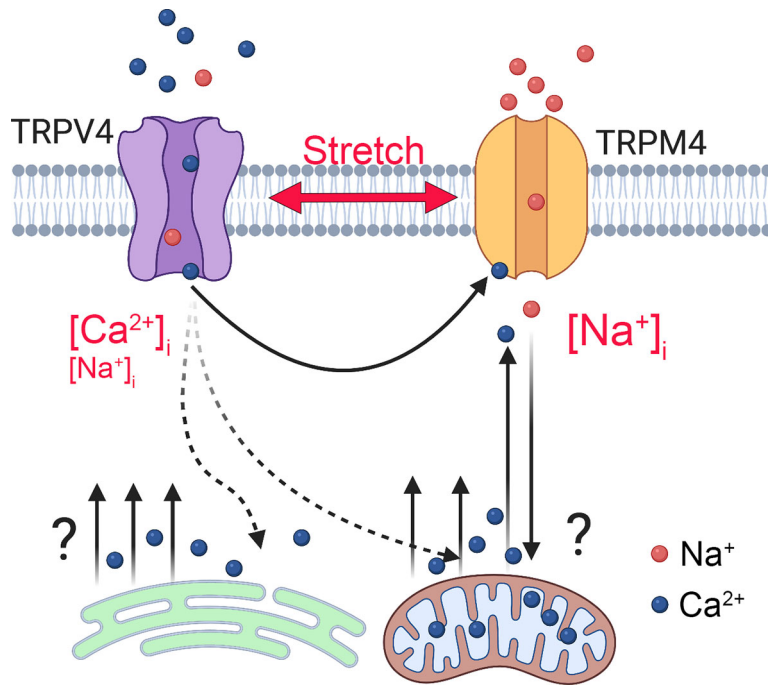


FIGURE 9 | Model of TRPM4-dependent calcium oscillations downstream from TRPV4. Mechanical stretch triggers cation influx through TRPV4 to elevate $[Ca^{2+}]_i$ and activate TRPM4, a Ca^{2+}-dependent Na^+ channel to depolarize the TM cells and increase $[Na^+]_i$. TRPM4 activation is required for voltage-independent oscillatory release of Ca^{2+} from a yet-unknown intracellular compartment.

events in human TM cells (62) and oscillatory phenotypes in TRPV4-expressing macrophages/monocytes, fibroblasts, keratinocytes, endothelial cells, chondrocytes, and glia (50, 55) that have been linked to cellular microcontractions, ECM remodeling and transfer of mechanical force across load-bearing focal adhesions (49, 50, 63). In macrophages, TRPM4 regulates cellular calcium oscillations and contractility *via* FAK and Rac GTPases (27, 53, 55), processes that may be downstream from TRPV4 (14; **Figure 4**). Together, these data implicate TRPV4-TRPM4 interactions in endogenous, cell-generated control of stretch-sensitive tyrosine phosphorylations, RhoA signaling and contractility. Another intriguing possibility is that TRPV4-dependent Ca^{2+} oscillations operate at the threshold of contractile, RhoA-dependent (14) vs. relaxing, nitric oxide-dependent (64) states associated with myogenic-like contractility (62, 65, 66). TRPM4 shares the regulatory sulphonylurea receptor (SUR1/2) with inward rectifying K^+ (Kir6.1 and Kir6.2) subunits that form K_{ATP} channels sensitive to $[Ca^{2+}]_i$ and intracellular ATP (67, 68) and regulate NFATc1 signaling in immune cells (39). The effect of K_{ATP} channel openers on intraocular pressure (69) could include parallel modulation of the SUR1-TRPM4 complex, Ca^{2+} and Na^+ homeostasis. The small, non-significant decrease in outflow facility in the presence of 9-PA and ocular normotension in mice with ablated TRPM4 gene suggest that TRPM4 is not required for steady-state IOP maintenance but it remains to be seen whether the contribution of TRPM4 channels can be unmasked under conditions associated with maximal TRPV4 activation.

In conclusion, our findings bring mechanistic evidence for novel interactions between mechanotransducers, TRPM4 channels and Ca^{2+} stores that may, in the presence of increased membrane strain, alter the cells' membrane potential together with intracellular $[Ca^{2+}]_i$ and $[Na^+]_i$. Analogy with other load-bearing and immune-like cells, suggests that a persistent pacemaking loop between Ca^{2+} influx, release and Ca^{2+}-activated channels downstream from TRPV4 could suggests that a time-dependently coordinate transcription factors, actomyosin-driven tension, mechanical load transfer across focal contacts, and secretion of matrix metalloproteinases. While investigations of TM biology typically focus on smooth muscle cell- and endothelial-like properties of resident cells, it is worth underscoring their role in IOP-dependent innate immune regulation in the anterior eye. Aqueous humor inhibits immune effector cells (70) and thus key phagocytic, scavenger and immune functions in the outflow pathway are relegated to TM cells (70–72), which express immune-like markers such as complement C1QB, the tyrosine kinase binding protein (TYROBP), major histocompatibility complex proteins and TLR4 (7, 64, 73, 74). We found that, similar to macrophages/monocytes and mast cells, TM cells utilize TRPM4 for oscillatory activity, which is triggered downstream from the TRPV4 channel that integrates mechanical, temperature and chemical inputs (15–17). This suggests that TRPM4-dependent calcium oscillations and their role in TLR4-dependent phagocytosis, cytokine production and survival (31, 32) might be informed by the biomechanical milieu. TLR4 signaling regulates TM TGFβ production (7) and has been linked to both TRPV4 and TRPM4 activation (19, 31, 39). Owing to their role in translayer Ca^{2+}, Na^+ and water transport dynamics, myofibroblast transformation and immune regulation, TRPV4-TRPM4 interactions could therefore be targeted by translational interventions aimed at fine-tuning the homeostatic functions of the conventional outflow pathway and regulation of intraocular pressure.

DATA AVAILABILITY STATEMENT

The original contributions presented in the study are included in the article/**Supplementary Material**. Further inquiries can be directed to the corresponding author.

ETHICS STATEMENT

The animal study was reviewed and approved by Institutional Animal Care and Use Committee - University of Utah.

AUTHOR CONTRIBUTIONS

OY, TP, FV, JB, Jv, SR, ML, CR and JB carried out the experiments. OY, JB, SR and Jv performed the statistical analyses. EH and MF provided reagents/animal models. OY and DK drafted the manuscript. OY, DO and DK conceived and coordinated the study. The authors read and approved the final manuscript.

FUNDING

Supported by, National Institutes of Health (R01EY027920, R01EY031817, P30EY014800, T32EY024234), Stauss-Rankin Foundation, USAMRAA (VR200079) and unrestricted support from Research to Prevent Blindness to the Moran Eye Institute at the University of Utah.

SUPPLEMENTARY MATERIAL

The Supplementary Material for this article can be found online at: https://www.frontiersin.org/articles/10.3389/fimmu.2022.805076/full#supplementary-material

Supplementary Figure 1 | Validation of TRPM4 shRNA constructs. **(A)** Typical WB results representing knockdown effects of the TRPM4 shRNA constructs in the HEK-293 overexpression system. **(B)** Quantification of results shown in (A). The results are representative of three independent experiments.

Supplementary Figure 2 | HEK293 cells. TRPV4 and TRPM4 coexpression is sufficient to sustain calcium oscillations in the presence of GSK101. Representative traces of ratiometric signals in **(A)** TRPV4 + TRPM4 DNA-transfected cells and **(B)** Cells transfected with TRPV4 alone. **(C)** Averaged frequency of $[Ca^{2+}]_i$ transients in TRPV4+TRPM4 expressing cells before and after GSK101 exposure.

REFERENCES

1. Coulombre AJ, Steinberg SN, Coulombre JL. The Role of Intraocular Pressure in the Development of the Chick Eye. V. Pigmented Epithelium. *Invest Ophthalmol* (1963) 2:83–9.
2. Acott TS, Kelley MJ, Keller KE, Vranka JA, Abu-Hassan DW, Li X, et al. Intraocular Pressure Homeostasis: Maintaining Balance in a High-Pressure Environment. *J Ocul Pharmacol Ther* (2014) 30:94–101. doi: 10.1089/jop.2013.0185
3. Bradley JM, Kelley MJ, Zhu X, Anderssohn AM, Alexander JP, Acott TS. Effects of Mechanical Stretching on Trabecular Matrix Metalloproteinases. *Invest Ophthalmol Vis Sci* (2001) 42:1505–13.
4. Rohen JW, Lütjen-Drecoll E, Flügel C, Meyer M, Grierson I. Ultrastructure of the Trabecular Meshwork in Untreated Cases of Primary Open-Angle Glaucoma (POAG). *Exp Eye Res* (1993) 56:683–92. doi: 10.1006/exer.1993.1085
5. Last JA, Pan T, Ding Y, Reilly CM, Keller K, Acott TS, et al. Elastic Modulus Determination of Normal and Glaucomatous Human Trabecular Meshwork. *Invest Ophthalmol Vis Sci* (2011) 52:2147–52. doi: 10.1167/iovs.10-6342
6. Patel G, Fury W, Yang H, Gomez-Caraballo M, Bai Y, Yang T, et al. Molecular Taxonomy of Human Ocular Outflow Tissues Defined by Single-Cell Transcriptomics. *Proc Natl Acad Sci USA* (2020) 117:12856–67. doi: 10.1073/pnas.2001896117
7. Hernandez H, Medina-Ortiz WE, Luan T, Clark AF, McDowell CM. Crosstalk Between Transforming Growth Factor Beta-2 and Toll-Like Receptor 4 in the Trabecular Meshwork. *Invest Ophthalmol Vis Sci* (2017) 58:1811–23. doi: 10.1167/iovs.16-21331
8. Poyomtip T. Roles of Toll-Like Receptor 4 for Cellular Pathogenesis in Primary Open-Angle Glaucoma: A Potential Therapeutic Strategy. *J Microbiol Immunol Infect* (2019) 52(2):201–6. doi: 10.1016/j.jmii.2018.12.006
9. Filla MS, Faralli JA, Peotter JL, Peters DM. The Role of Integrins in Glaucoma. *Exp Eye Res* (2017) 158:124–36. doi: 10.1016/j.exer.2016.05.011
10. Yarishkin O, Phuong TTT, Bretz CA, Olsen KW, Baumann JM, Lakk M, et al. TREK-1 Channels Regulate Pressure Sensitivity and Calcium Signaling in Trabecular Meshwork Cells. *J Gen Physiol* (2018) 150:1660–75. doi: 10.1085/jgp.201812179
11. Yarishkin O, Phuong TTT, Baumann JM, De Ieso ML, Vazquez-Chona F, Rudzitis CN, et al. Piezo1 Channels Mediate Trabecular Meshwork Mechanotransduction and Promote Aqueous Fluid Outflow. *J Physiol* (2021) 599:571–92. doi: 10.1113/JP281011
12. Luo N, Conwell MD, Chen X, Kettenhofen CI, Westlake CJ, Cantor LB, et al. Primary Cilia Signaling Mediates Intraocular Pressure Sensation. *Proc Natl Acad Sci U.S.A.* (2014) 111:12871–6. doi: 10.1073/pnas.1323292111
13. Ryskamp DA, Frye AM, Phuong TTT, Yarishkin O, Jo AO, Xu Y, et al. TRPV4 Regulates Calcium Homeostasis, Cytoskeletal Remodeling, Conventional Outflow and Intraocular Pressure in the Mammalian Eye. *Sci Rep* (2016) 6:30585. doi: 10.1038/srep30583
14. Lakk M, Križajs D. TRPV4-Rho Signaling Drives Cytoskeletal and Focal Adhesion Remodeling in Trabecular Meshwork Cells. *Am J Physiol - Cell Physiol* (2021) 320:C1013–30. doi: 10.1152/ajpcell.00599.2020
15. Križaj D. *What is Glaucoma? Webvision Organ Retin Vis Syst*. Salt Lake City: University of Utah Health Sciences Center (2019).
16. White JPM, Cibelli M, Urban L, Nilius B, McGeown JG, Nagy I. TRPV4: Molecular Conductor of a Diverse Orchestra. *Physiol Rev* (2016) 96:911–73. doi: 10.1152/physrev.00016.2015
17. Berna-Erro A, Izquierdo-Serra M, Sepúlveda RV, Rubio-Moscardo F, Doñate-Macián P, Serra SA, et al. Structural Determinants of 5',6'-Epoxyeicosatrienoic Acid Binding to and Activation of TRPV4 Channel. *Sci Rep* (2017) 7:10522. doi: 10.1038/s41598-017-11274-1
18. Thibodeau ML, Peters CH, Townsend KN, Shen Y, Hendson G, Adam S, et al. Compound Heterozygous TRPV4 Mutations in Two Siblings With a Complex Phenotype Including Severe Intellectual Disability and Neuropathy. *Am J Med Genet A* (2017) 173:3087–92. doi: 10.1002/ajmg.a.38400
19. Rahaman SO, Grove LM, Paruchuri S, Southern BD, Abraham S, Niese KA, et al. TRPV4 Mediates Myofibroblast Differentiation and Pulmonary Fibrosis in Mice. *J Clin Invest* (2014) 124:5225–38. doi: 10.1172/JCI75331
20. Sharma S, Goswami R, Rahaman SO. The TRPV4-TAZ Mechanotransduction Signaling Axis in Matrix Stiffness- and Tgfβ1-Induced Epithelial-Mesenchymal Transition. *Cell Mol Bioeng* (2019) 12:139-52. doi: 10.1007/s12195-018-00565-w
21. Lorenzo IM, Liedtke W, Sanderson MJ, Valverde MA. TRPV4 Channel Participates in Receptor-Operated Calcium Entry and Ciliary Beat Frequency Regulation in Mouse Airway Epithelial Cells. *Proc Natl Acad Sci USA* (2008) 105:12611–6. doi: 10.1073/pnas.0803970105
22. Goswami C, Kuhn J, Heppenstall PA, Hucho T. Importance of non-Selective Cation Channel TRPV4 Interaction With Cytoskeleton and Their Reciprocal Regulations in Cultured Cells. *PloS One* (2010) 5:e11654. doi: 10.1371/journal.pone.0011654
23. Jo AO, Ryskamp DA, Phuong TTT, Verkman AS, Yarishkin O, Macaulay N. Križaj D. TRPV4 and AQP4 Channels Synergistically Regulate Cell Volume and Calcium Homeostasis in Retinal Müller Glia. *J Neurosci* (2015) 35:13525–73. doi: 10.1523/JNEUROSCI.1987-15.2015
24. Li P, Bian X, Liu C, Wang S, Guo M, Tao Y, et al. STIM1 and TRPV4 Regulate Fluid Flow-Induced Calcium Oscillation at Early and Late Stages of Osteoclast Differentiation. *Cell Calcium* (2018) 71:45–52. doi: 10.1016/j.ceca.2017.12.001
25. Voets T, Prenen J, Vriens J, Watanabe H, Janssens A, Wissenbach U, et al. Molecular Determinants of Permeation Through the Cation Channel TRPV4. *J Biol Chem* (2002) 277:33704–10. doi: 10.1074/jbc.M204828200
26. Guinamard R, Demion M, Magaud C, Potreau D, Bois P. Functional Expression of the TRPM4 Cationic Current in Ventricular Cardiomyocytes From Spontaneously Hypertensive Rats. *Hypertension* (2006) 48:587–94. doi: 10.1161/01.HYP.0000237864.65019.a5
27. Launay P, Cheng H, Srivatsan S, Penner R, Fleig A, Kinet JP. TRPM4 Regulates Calcium Oscillations After T Cell Activation. *Science* (2004) 306:1374–77. doi: 10.1126/science.1098845
28. Burt R, Graves BM, Gao M, Li C, Williams DL, Fregoso SP, et al. 9-Phenanthrol and Flufenamic Acid Inhibit Calcium Oscillations in HL-1 Mouse Cardiomyocytes. *Cell Calcium* (2013) 54:193–201. doi: 10.1016/j.ceca.2013.06.003
29. Simard C, Sallé L, Rouet R, Guinamard R. Transient Receptor Potential Melastatin 4 Inhibitor 9-Phenanthrol Abolishes Arrhythmias Induced by Hypoxia and Re-Oxygenation in Mouse Ventricle. *Br J Pharmacol* (2012) 165:2354–64. doi: 10.1111/j.1476-5381.2011.01715.x
30. Jo AO, Lakk M, Frye AM, Phuong TT, Redmon SN, Roberts R, et al. Differential Volume Regulation and Calcium Signaling in Two Ciliary Body Cell Types is Subserved by TRPV4 Channels. *Proc Natl Acad Sci U.S.A.* (2016) 113:3885–90. doi: 10.1073/pnas.1515895113
31. Serafini N, Dahdah A, Barbet G, Demion M, Attout T, Gautier G, et al. The TRPM4 Channel Controls Monocyte and Macrophage, But Not Neutrophil, Function for Survival in Sepsis. *J Immunol* (2012) 189:3689–99. doi: 10.4049/jimmunol.1102969
32. Scheraga RG, Abraham S, Niese KA, Southern BD, Grove LM, Hite RD, et al. TRPV4 Mechanosensitive Ion Channel Regulates Lipopolysaccharide-Stimulated Macrophage Phagocytosis. *J Immunol* (2016) 196:428–36. doi: 10.4049/jimmunol.1501688
33. Lakk M, Yarishkin O, Baumann JM, Iuso A, Križaj D. Cholesterol Regulates Polymodal Sensory Transduction in Müller Glia. *Glia* (2017) 65:2038–50. doi: 10.1002/glia.23213
34. Redmon SN, Yarishkin O, Lakk M, Jo A, Mustafić E, Tvrdik P, et al. TRPV4 Channels Mediate the Mechanoresponse in Retinal Microglia. *Glia* (2021) 69:1563–82. doi: 10.1002/glia.23979
35. Molnár T, Yarishkin O, Iuso A, Barabas P, Jones B, Marc RE, et al. Store-Operated Calcium Entry in Müller Glia is Controlled by Synergistic Activation of TRPC and Orai Channels. *J Neurosci* (2016) 36:3184–98. doi: 10.1523/JNEUROSCI.4069-15.2016
36. Yarishkin O, Phuong TTT, Križaj D. Trabecular Meshwork TREK-1 Channels Function as Polymodal Integrators of Pressure and pH. *Investig Ophthalmol Vis Sci* (2019) 60:2294–303. doi: 10.1167/iovs.19-26851
37. Sherwood JM, Reina-Torres E, Bertrand JA, Rowe B, Overby DR. Measurement of Outflow Facility Using Iperfusion. *PloS One* (2016) 11:e0150694. doi: 10.1371/journal.pone.0150694
38. Sherwood JM, Boazak EM, Feola AJ, Parker K, Ethier CR, Overby DR. Measurement of Ocular Compliance Using Iperfusion. *Front Bioeng Biotechnol* (2019) 7:276. doi: 10.3389/fbioe.2019.00276
39. Kurland DB, Gerzanich V, Karimy JK, Woo SK, Vennekens R, Freichel M, et al. The Sur1-Trpm4 Channel Regulates NOS2 Transcription in TLR4-Activated Microglia. *J Neuroinflamm* (2016) 13(1):130. doi: 10.1186/s12974-016-0599-2

40. Earley S, Waldron BJ, Brayden JE. Critical Role for Transient Receptor Potential Channel TRPM4 in Myogenic Constriction of Cerebral Arteries. *Circ Res* (2004) 95:922–9. doi: 10.1161/01.RES.0000147311.54833.03
41. Akopian A, Križaj D, Witkovsky P. Both High- and Low Voltage-Activated Calcium Currents Contribute to the Light-Evoked Responses of Luminosity Horizontal Cells in the Xenopus Retina. *Brain Res* (1997) 762:121–30. doi: 10.1016/S0006-8993(97)00374-0
42. Yarishkin OV, Hwang EM, Kim D, Yoo JC, Kang SS, Kim DR, et al. Diclofenac, a Non-Steroidal Anti-Inflammatory Drug, Inhibits L-Type Ca Channels in Neonatal Rat Ventricular Cardiomyocytes. *Korean J Physiol Pharmacol* (2009) 13:437–42. doi: 10.4196/kjpp.2009.13.6.437
43. Križaj D, Bao JX, Schmitz Y, Witkovsky P, Copenhagen DR. Caffeine-Sensitive Calcium Stores Regulate Synaptic Transmission From Retinal Rod Photoreceptors. *J Neurosci* (1999) 19:7249–61. doi: 10.1523/jneurosci.19-17-07249.1999
44. Grand T, Demion M, Norez C, Mettey Y, Launay P, Becq F, et al. 9-Phenanthrol Inhibits Human TRPM4 But Not TRPM5 Cationic Channels. *Br J Pharmacol* (2008) 153:1697–705. doi: 10.1038/bjp.2008.38
45. Guinamard R, Hof T, Del Negro CA. The TRPM4 Channel Inhibitor 9-Phenanthrol. *Br J Pharmacol* (2014) 171:1600–13. doi: 10.1111/bph.12582
46. Demion M, Bois P, Launay P, Guinamard R. TRPM4, a Ca2+-Activated Nonselective Cation Channel in Mouse Sino-Atrial Node Cells. *Cardiovasc Res* (2007) 73:531–8. doi: 10.1016/j.cardiores.2006.11.023
47. Yarishkin OV, Hwang EM, Park JY, Kang D, Han J, Hong SG. Endogenous TRPM4-Like Channel in Chinese Hamster Ovary (CHO) Cells. *Biochem Biophys Res Commun* (2008) 369:712–7. doi: 10.1016/j.bbrc.2008.02.081
48. Park JY, Hwang EM, Yarishkin O, Seo JH, Kim E, Yoo J, et al. TRPM4b Channel Suppresses Store-Operated Ca2+ Entry by a Novel Protein-Protein Interaction With the TRPC3 Channel. *Biochem Biophys Res Commun* (2008) 368:677–83. doi: 10.1016/j.bbrc.2008.01.153
49. Holmes DF, Yeung C-YC, Garva R, Zindy E, Taylor SH, Lu Y, et al. Synchronized Mechanical Oscillations at the Cell-Matrix Interface in the Formation of Tensile Tissue. *Proc Natl Acad Sci USA* (2018) 115:E9288–97. doi: 10.1073/pnas.1801759115
50. Gilchrist CL, Leddy HA, Kaye L, Case ND, Rothenberg KE, Little D, et al. TRPV4-Mediated Calcium Signaling in Mesenchymal Stem Cells Regulates Aligned Collagen Matrix Formation and Vinculin Tension. *Proc Natl Acad Sci USA* (2019) 116:1992–7. doi: 10.1073/pnas.1811095116
51. Piao H, Takahashi K, Yamaguchi Y, Wang C, Liu K, Naruse K. Transient Receptor Potential Melastatin-4 is Involved in Hypoxia-Reoxygenation Injury in the Cardiomyocytes. *PloS One* (2015) 10:e0121703. doi: 10.1371/journal.pone.0121703
52. Stokum JA, Kwon MS, Woo SK, Tsymbalyuk O, Vennekens R, Gerzanich V, et al. SUR1-TRPM4 and AQP4 Form a Heteromultimeric Complex That Amplifies Ion/Water Osmotic Coupling and Drives Astrocyte Swelling. *Glia* (2018) 66:108–25. doi: 10.1002/glia.23231
53. Launay P, Fleig A, Perraud AL, Scharenberg AM, Penner R, Kinet JP. TRPM4 is a Ca2+-Activated Nonselective Cation Channel Mediating Cell Membrane Depolarization. *Cell* (2002) 109:531–8. doi: 10.1016/S0092-8674(02)00719-5
54. Vennekens R, Nilius B. Insights Into TRPM4 Function, Regulation and Physiological Role. *Handb Exp Pharmacol* (2007) 179:269–85. doi: 10.1007/978-3-540-34891-7_16
55. Cáceres M, Ortiz L, Recabarren T, Romero A, Colombo A, Leiva-Salcedo E, et al. TRPM4 Is a Novel Component of the Adhesome Required for Focal Adhesion Disassembly, Migration and Contractility. *PloS One* (2015) 10:e0130540. doi: 10.1371/journal.pone.0130540
56. Gerzanich V, Kwon MS, Woo SK, Ivanov A, Simard JM. SUR1-TRPM4 Channel Activation and Phasic Secretion of MMP-9 Induced by tPA in Brain Endothelial Cells. *PloS One* (2018) 13:e0195526. doi: 10.1371/journal.pone.0195526
57. O'Malley JJ, Seibt F, Chin J, Beierlein M. TRPM4 Conductances in Thalamic Reticular Nucleus Neurons Generate Persistent Firing During Slow Oscillations. *J Neurosci* (2020) 40:4813–23. doi: 10.1523/JNEUROSCI.0324-20.2020
58. Garcia-Elias A, Lorenzo IM, Vicente R, Valverde MA. IP3 Receptor Binds to and Sensitizes TRPV4 Channel to Osmotic Stimuli *via* a Calmodulin-Binding Site. *J Biol Chem* (2008) 283:31284–8. doi: 10.1074/jbc.C800184200
59. Morita H, Honda A, Inoue R, Ito Y, Abe K, Nelson MT, et al. Membrane Stretch-Induced Activation of a TRPM4-Like Nonselective Cation Channel in Cerebral Artery Myocytes. *J Pharmacol Sci* (2007) 103:417–26. doi: 10.1254/jphs.fp0061332
60. Gonzales AL, Yang Y, Sullivan MN, Sanders L, Dabertrand F, Hill-Eubanks DC, et al. A Plcγ1-Dependent, Force-Sensitive Signaling Network in the Myogenic Constriction of Cerebral Arteries. *Sci Signal* (2014) 7:ra49. doi: 10.1126/scisignal.2004732
61. Constantine M, Liew CK, Lo V, Macmillan A, Cranfield CG, Sunde M, et al. Heterologously-Expressed and Liposome-Reconstituted Human Transient Receptor Potential Melastatin 4 Channel (TRPM4) is a Functional Tetramer. *Sci Rep* (2016) 6:19352. doi: 10.1038/srep19352
62. Matsuo T, Matsuo N. Intracellular Calcium Response to Hydraulic Pressure in Human Trabecular Cells. *Br J Ophthalmol* (1996) 80:561–6. doi: 10.1136/bjo.80.6.561
63. Castella LF, Buscemi L, Godbout C, Meister J-J, Hinz B. A New Lock-Step Mechanism of Matrix Remodelling Based on Subcellular Contractile Events. *J Cell Sci* (2010) 123:1751–60. doi: 10.1242/jcs.066795
64. Patel PD, Chen Y-L, Kasetti RB, Maddineni P, Mayhew W, Millar JC, et al. Impaired TRPV4-eNOS Signaling in Trabecular Meshwork Elevates Intraocular Pressure in Glaucoma. *Proc Natl Acad Sci USA* (2021) 118:e2022461118. doi: 10.1073/pnas.2022461118
65. Wiederholt M, Thieme H, Stumpff F. The Regulation of Trabecular Meshwork and Ciliary Muscle Contractility. *Prog Retin Eye Res* (2000) 19:271–95. doi: 10.1016/s1350-9462(99)00015-4
66. Guinamard R, Demion M, Chatelier A, Bois P. Calcium-Activated Nonselective Cation Channels in Mammalian Cardiomyocytes. *Trends Cardiovasc Med* (2006) 16:245–50. doi: 10.1016/j.tcm.2006.04.007
67. Guinamard R, Demion M, Launay P. Physiological Roles of the TRPM4 Channel Extracted From Background Currents. *Physiol (Bethesda)* (2010) 25:155–64. doi: 10.1152/physiol.00004.2010
68. Woo SK, Tsymbalyuk N, Tsymbalyuk O, Ivanova S, Gerzanich V, Simard JM. SUR1-TRPM4 Channels, Not KATP, Mediate Brain Swelling Following Cerebral Ischemia. *Neurosci Lett* (2020) 718:108–25. doi: 10.1016/j.neulet.2019.134729
69. Chowdhury UR, Holman BH, Fautsch MP. ATP-Sensitive Potassium (K(ATP)) Channel Openers Diazoxide and Nicorandil Lower Intraocular Pressure. *vivo Invest Ophthalmol Vis Sci* (2013) 54:4892–9. doi: 10.1167/iovs.13-11872
70. Streilein JW. Ocular Immune Privilege: Therapeutic Opportunities From an Experiment of Nature. *Nat Rev Immunol* (2003) 3:879–88. doi: 10.1038/nri1224
71. Biros D. Anterior Chamber-Associated Immune Deviation. *Vet Clin North Am - Small Anim Pract* (2008) 38:309–21. doi: 10.1016/j.cvsm.2007.12.006
72. Latina M. Immunohistochemical Staining of the Human Anterior Segment. *Arch Ophthalmol* (1988) 106:95–9. doi: 10.1001/archopht.1988.01060130101037
73. Tripathi BJ, Tripathi RC, Wong P, Raja S. Expression of HLA by the Human Trabecular Meshwork and Corneal Endothelium. *Exp Eye Res* (1990) 51:269–76. doi: 10.1016/0014-4835(90)90023-N
74. Grybauskas A, Koga T, Kuprys PV, Nolan M, McCarty R, Walker L, et al. ABCB1 Transporter and Toll-Like Receptor 4 in Trabecular Meshwork Cells. *Mol Vis* (2015) 21:201–12.

Conflict of Interest: The authors declare that the research was conducted in the absence of any commercial or financial relationships that could be construed as a potential conflict of interest

Publisher's Note: All claims expressed in this article are solely those of the authors and do not necessarily represent those of their affiliated organizations, or those of the publisher, the editors and the reviewers. Any product that may be evaluated in this article, or claim that may be made by its manufacturer, is not guaranteed or endorsed by the publisher.

Copyright © 2022 Yarishkin, Phuong, Vazquez-Chona, Bertrand, van Battenburg-Sherwood, Redmon, Rudzitis, Lakk, Baumann, Freichel, Hwang, Overby and Križaj. This is an open-access article distributed under the terms of the Creative Commons Attribution License (CC BY). The use, distribution or reproduction in other forums is permitted, provided the original author(s) and the copyright owner(s) are credited and that the original publication in this journal is cited, in accordance with accepted academic practice. No use, distribution or reproduction is permitted which does not comply with these terms.